Bulletin of the Seismological Society of America, 90, 3, pp. 702–708, June 2000

Seismological Studies at Parkfield VIII: Modeling the Observed Travel-Time Changes

by V. A. Korneev, T. V. McEvilly, and E. D. Karageorgi

Abstract For 10 years, as one element of the Parkfield, California, Prediction Experiment, the borehole seismographic network was illuminated routinely by a large shear-wave Vibroseis from several source points to investigate the stability of wave propagation in the fault zone and the possibility of nucleation-related premonitory phenomena. Clear and progressive travel-time changes of up to 50 msec were detected during the study, most prominent in the *S*-wave coda, and localized to propagation paths through the shallow fault zone (above about 500 m depth) southeast of Middle Mountain, the section of the fault where previous *M* 6 earthquakes have initiated. We model the observations successfully as interaction (reflection and transmission) of the shallow wavefield with a 200-meter-wide low-velocity fault zone in which the velocity increases by 6%, due, we hypothesize, to hydrological changes accompanying a significant pulse in fault slip rate and seismicity.

Introduction

A unique data set for the study of wave propagation in the San Andreas fault zone has been acquired in the Parkfield Prediction Experiment underway in central California (Bakun and Lindh, 1985). Data have been collected with a 10-station borehole network in a search for evidence of changes in seismicity, seismic velocity, or waveforms associated with the nucleation process of the anticipated *M* 6 earthquake at Parkfield (see Karageorgi *et al.,* 1992, for the network description). More than 6000 earthquakes have been recorded since 1987 in the magnitude range $-1 < M < 5$. In addition, seismograms for 720 source-receiver paths have been obtained for repeated illumination (56 times) of the network using a large shear-wave Vibroseis, from June, 1987, until December, 1996, when that element of the program ended (Karageorgi *et al.,* 1992, 1997). That investigation reported significant travel-time changes in the *S*-wave coda for paths crossing the fault zone southeast from the epicenter of the 1966 *M* 6 earthquake. Systematic travel-time changes up to 50 msec were seen in the anomalous region during the study. The same waveforms that experienced travel-time changes also exhibited changes in frequency content and polarization. The affected region includes the zone of nucleation and rupture onset for the previous *M* 6 Parkfield earthquakes, and, possibly, the region of slip initiation for the great southern California earthquake of 1857 (Sieh, 1978). Temporal patterns in the variations appeared to be synchronous with observed changes in deformation and seismicity (Karageorgi *et al.,* 1997; Nadeau and McEvilly, 1999). Similar variations in travel times or coda-Q were not seen for more deeply propagating waveforms recorded from microearthquakes on the same segment of the fault (Nadeau *et al.,* 1994a, 1994b; Antolik *et al.,* 1996), prompting Karageorgi *et al.* (1997) to hypothesize that changing fluid conditions in the uppermost section of the fault zone, in response to deeper tectonic stress perturbations, were responsible for the changes detected in the Vibroseis monitoring program. To explore this shallow fluids hypothesis more quantitatively, in this study we model the observed waveform changes numerically using plausible velocity perturbations in the shallow fault zone.

The Study Region and Data Set

At Parkfield the San Andreas fault zone is a striking near-vertical low-velocity zone, and it very clearly acts as a waveguide for seismic energy from earthquakes on the fault and from surface sources (Li *et al.,* 1997; Korneev *et al.,* 1998). Velocity models there show high *Vp*/*Vs* ratio along the fault near the surface and at depth within the fault zone, and a pronounced strong vertical velocity gradient in the upper 2 km of the section (Michelini and McEvilly, 1991; Eberhart-Phillips and Michael, 1993). *P*- and *S*-wave velocity models show an approximately two-dimensional structure in the region of the travel-time anomaly.

Figure 1 shows the central portion of the Parkfield study region. Seven of the ten borehole seismometer sites and five of the eight vibrator sites (VPs) lie within this map area. The region of anomalous waveform changes lies along the fault zone in the lower half of the map, southeastward from the MMN station. Karageorgi *et al.* (1992, 1997) used data from all of the VPs and receivers to define the anomalous region

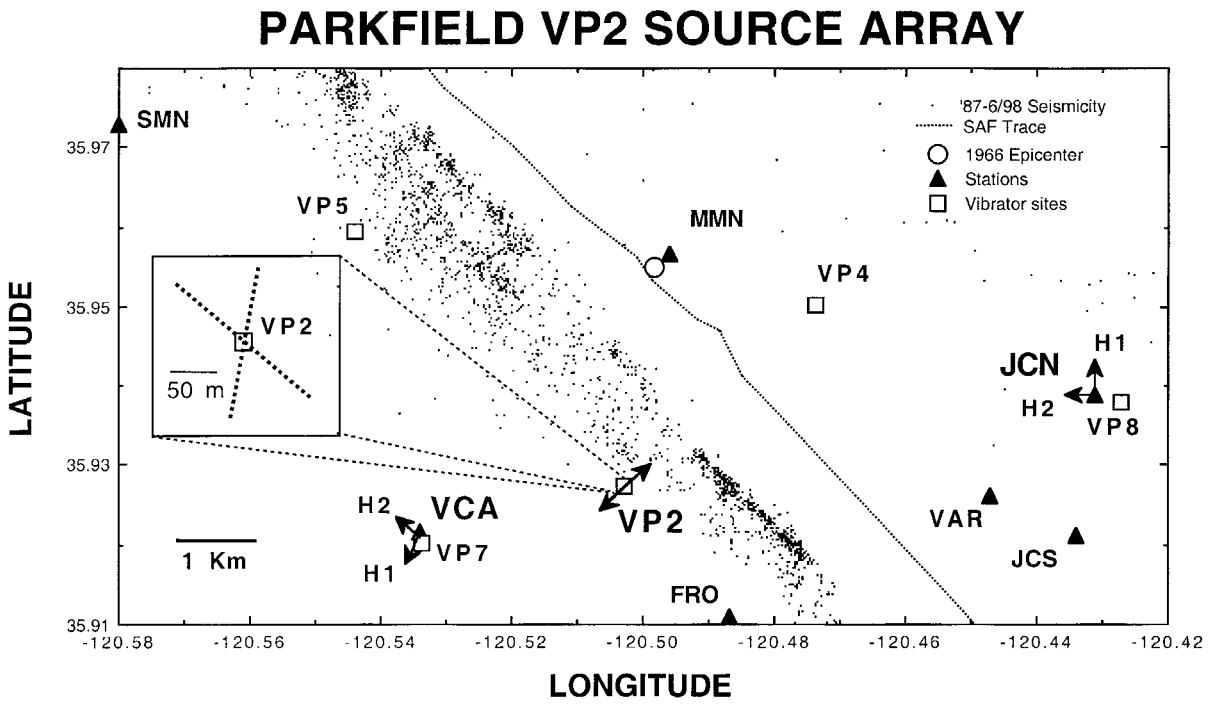

Figure 1. Central region of the Parkfield experiment showing VPs and receiving stations. Data from VP2 point source and from the fault-parallel arm of the VP2 source array recorded at stations VCA and JCN are the focus of this modeling study. The region in which the travel-time changes were seen in the *S* coda for many source-receiver paths begins around station MMN and extends to the southeast along the fault zone. The VP2 source array contained 17 VPs at 10-m spacing, and the shear-wave vibrator was oriented to generate a fault-normal polarization of the *S* wave (arrow at VP2). Orientations of the horizontal-component geophones H1 and H2 at VCA and JCN are indicated by arrows.

of travel-time variation. At VP2, in addition to the routine point-source monitoring data, a cross array of sources with 17 VPs on each leg was deployed (see insert in Figure 1), but only once, for the purpose of determining the frequency-wavenumber properties of coherent waveforms recorded throughout the network (see Karageorgi *et al.,* 1997) in an attempt to better define the complex nature of wave propagation in the heterogeneous region along the fault zone. A very complicated propagation geometry was revealed, presumably due to a combination of effects from the severe topographic variations and heterogeneity within the fault zone.

In this study we use the NW–SE oriented fault-parallel arm of the VP2 source array with fault-normal excitation of the shear-wave vibrator and seismograms recorded at stations VCA and JCN. These data represent energy propagating along source-receiver paths in the region where the travel-time variations were found.

Computational Approach

We attempt to explain the observed temporal changes in travel times reported by Karageorgi *et al.* (1997) for the VP2 point-source monitoring data recorded at VCA and JCN, using a numerical simulation of their hypothesized hydrological mechanism in the shallow fault zone. The two paths from VP2 to VCA and JCN are approximately colinear, and they sample segments of similar length on the two sides of the fault zone. We rely on the approximately fault-normal geometry of the paths to justify two-dimensional modeling of wave propagation as *P-SV* energy along those paths. The source array at VP2 reveals coherent arrivals in the wavefield that are helpful in interpreting the recorded seismograms.

Figure 2 shows the model geometry and numerical results. Receivers are in boreholes at depths of 200 and 224 m below the surface for VCA and JCN, respectively. The velocity profiles shown and used in our numerical simulation were derived from existing tomographic velocity models for the region. A major factor controlling the character of wave propagation at short distances from a surface source is the nature of the shallow vertical velocity gradient. For this exercise we approximated the velocity gradients from Michelini and McEvilly (1991) with a function of the form $V(z) = a + b\tan^{-1}(gz)$ and used the Vp/Vs ratio of 2.0 from the tomographic analyses. The gradient parameters a, b, and g

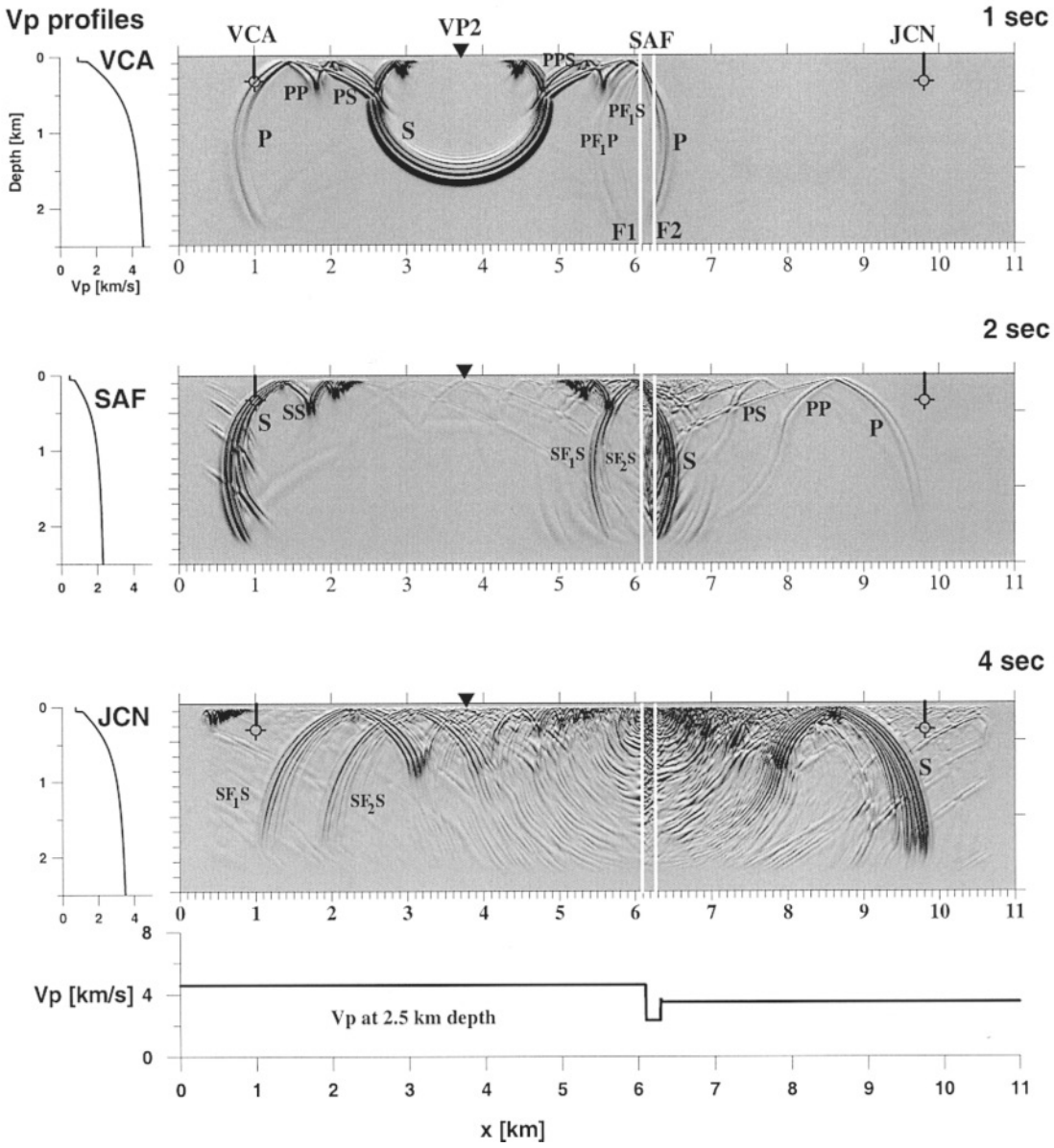

Figure 2. Velocity model and *P-SV* elastic wavefield computation in a 2D simulation of Vibroseis excitation at VP2 and propagation in a section through borehole stations VCA and JCN. Snapshots of the developing field are shown for lapse times of 1, 2, and 4 seconds. Interfaces F1 and F2 bound the fault zone (SAF). *P* waves pass VCA and the SAF at about 1 second, and the S waves are there by 2 seconds. At 2 seconds, the SAF is contributing scattered energy to the *P* coda on its way to JCN. At 4 seconds, fault-zone reflected waves SF_1S and SF_2S are approaching VCA, and SAF-scattered energy is building the shallow late coda of *S* that will be seen at both VCA and JCN. Trapped fault-zone guided-wave energy is also apparent.

for the VP2–VCA path were estimated to be 1.5 km/sec, 3.5 km/sec and 2.0 km^{-1}, respectively, by matching the observed and computed arrival times for direct arrivals in the early part of the VCA seismograms, prior to arrival of energy that interacted with the fault zone. Direct arrivals at JCN could be matched with velocity profiles for the NE side of the fault and for the narrow fault zone that are scaled reductions to 0.76 and 0.5 of the VCA values, respectively. The fault zone was modeled as a layer of thickness 200 meters, bounded by the interfaces F1 and F2 in the figure. The three velocity profiles determined in this manner produce the observed direct *P* and *S* arrival times at the two stations, and they are reasonably consistent with the tomographic models. The horizontal velocity profile at 2.5 km depth is also shown

in the figure. The model was digitized on a 2200 × 500 grid with 5 m spacing, yielding the 11 × 2.5 km section in Figure 2.

Computations were performed using a two-dimensional elastic finite-difference formulation with a staggered grid, an approach similar to the displacement-potential algorithm of Cao and Greenhalgh (1992). It employs two sets of equations with second-order spatial derivatives. Absorbing boundaries were simulated by damping boundary layers through exponentially changing properties. A gaussian-derivative-shaped source function with central frequency of 25 Hz was convolved with the computed traces to emulate the Vibroseis data. Resolution was maintained at better than 1/6 wavelength, and the equivalent small time steps allowed us to identify and track individual propagating phases in a "movie-like" detailed presentation of the developing wavefield.

Numerical results are illustrated in Figure 2, where the elastic wavefield development is presented in a series of three snapshots through time as the complex wave propagation evolves. Two features dominate the process: energy trapped near the surface by the shallow gradient, and wavefield scattering from the fault zone. Most of the energy is confined to the upper part of the section in multiple reflections at the free surface, producing a complex train of surface-guided waves made up of many arriving phases. In the synthetic wavefield, direct *P* and *S* waves arrive at VCA around 1 sec and 2 sec, respectively. At JCN they are seen at 2.2 sec and 4.4 sec. Because the receivers are located at depth, both up- and down-going energy is sensed, as well as horizontally propagating turning-point waves. The influence of the fault zone and shallow velocity gradient on the wavefield is dramatic. In the interval between the first-arriving *P* and *S* waves at VCA are the surface-generated multiples and converted phases. The latter are especially strong for *P* waves, e.g., *PS*, *PPS*.

In Figure 3 we analyze these computational results for their implications on travel-time changes observed along the two paths. In Figure 3a we show the actual seismograms produced by the VP2 array, for the fault-normal horizontal vibrator source along the fault-parallel (NW–SE) leg of the array. Two components of observed ground motion are presented, along with the 2D synthetic seismograms (*P-SV* motion; see Figure 2) at VCA and JCN. In Figure 3b we identify the principal direct and reflected arrivals in the synthetic traces and argue that the model produces a reasonable match to the observed wavefields at the two recording sites. Reflections seen at VCA are produced by the fault-zone boundaries, F1 and F2. PF_1P, the first F1 reflection at VCA, is small and masked by the large direct *S* wave just before it. F2 reflections at VCA have passed twice through the fault zone, and these late phases, such as PF_2PP (3.5 sec) and SF_2S (4.7 sec), are quite evident at the relative amplitude scale used in Figure 3b, arriving well after the direct waves have passed. In the trace-normalized presentation of Figure 3a these arrivals are much smaller in both observed and synthetic traces, but they nevertheless make up that part of the wavefield showing the large observed travel-time changes. At JCN the internal fault-zone reflections produce sequences of strong, distinct arrivals following the direct *P* and *S* waves. The time advance introduced by the velocity increase in the fault zone begins with the first *P* arrival at JCN, while at VCA it is not seen until the first fault-zone reflection arrives from F2. This characteristic is a critical test of the proposed model for the observed travel-time variations. The difference traces presented in Figure 3b represent simple subtraction of the reference trace from the variation trace (calculated for the velocity increase in the fault zone), and they show where the travel-time changes are to be expected. To emulate the analysis method of Karageorgi *et al.* (1992), we processed the computed reference and variation seismogram pairs with the same cross-correlation procedure they used to measure travel-time changes in the monitoring experiment. The resulting patterns of travel-time advances are presented in Figure 3c.

Intervals in the synthetic seismograms where large travel-time changes were observed at VCA and JCN in the monitoring project contain significant energy that is scattered from the fault zone. Our modeling results suggest a ready explanation for the cause of the progressively decreasing travel times reported by Karageorgi *et al.* (1997). For the path VP2–VCA, the changes were seen at arrival times after 3.5 sec, or, for our synthetic seismograms, after the direct waves had passed and the fault-zone reflected waves arrive. On the other hand, the observed travel-time changes for the VP2–JCN fault-crossing path begin immediately with the arrival of the direct *P* wave and increase continuously through the entire seismogram. The computed travel-time changes shown in Figure 3c exhibit these features. We take these results to be strong support for the proposition that the travel-time instabilities reported by Karageorgi *et al.* (1997) were most likely caused by changes in physical properties confined to the fault zone.

A direct comparison of the computed travel-time changes with the Vibroseis data is presented in Figure 4, where the synthetic-derived travel-time variations are superimposed on the Karageorgi *et al.* (1997) figure of observed travel-time shifts at both stations. The match is good. The first unstable wavelet at VCA corresponds to the PF_2PP reflection from the fault zone. At JCN, the anomaly onset coincides with the *P*-wave arrival, and the subsequent increase in travel-time advance is clear. In our numerical simulation this is due to progressive involvement of the slower *S* waves. The magnitude of the calculated travel-time variations match the observed data closely, and we consider the fault-zone velocity increase model to be supported by our analysis. It is important to point out that the 200 m and 6 % thickness-velocity change pair used in our modeling is not unique; other combinations can be found to match the observations. However, most such alternative models do not differ greatly from the one we have used.

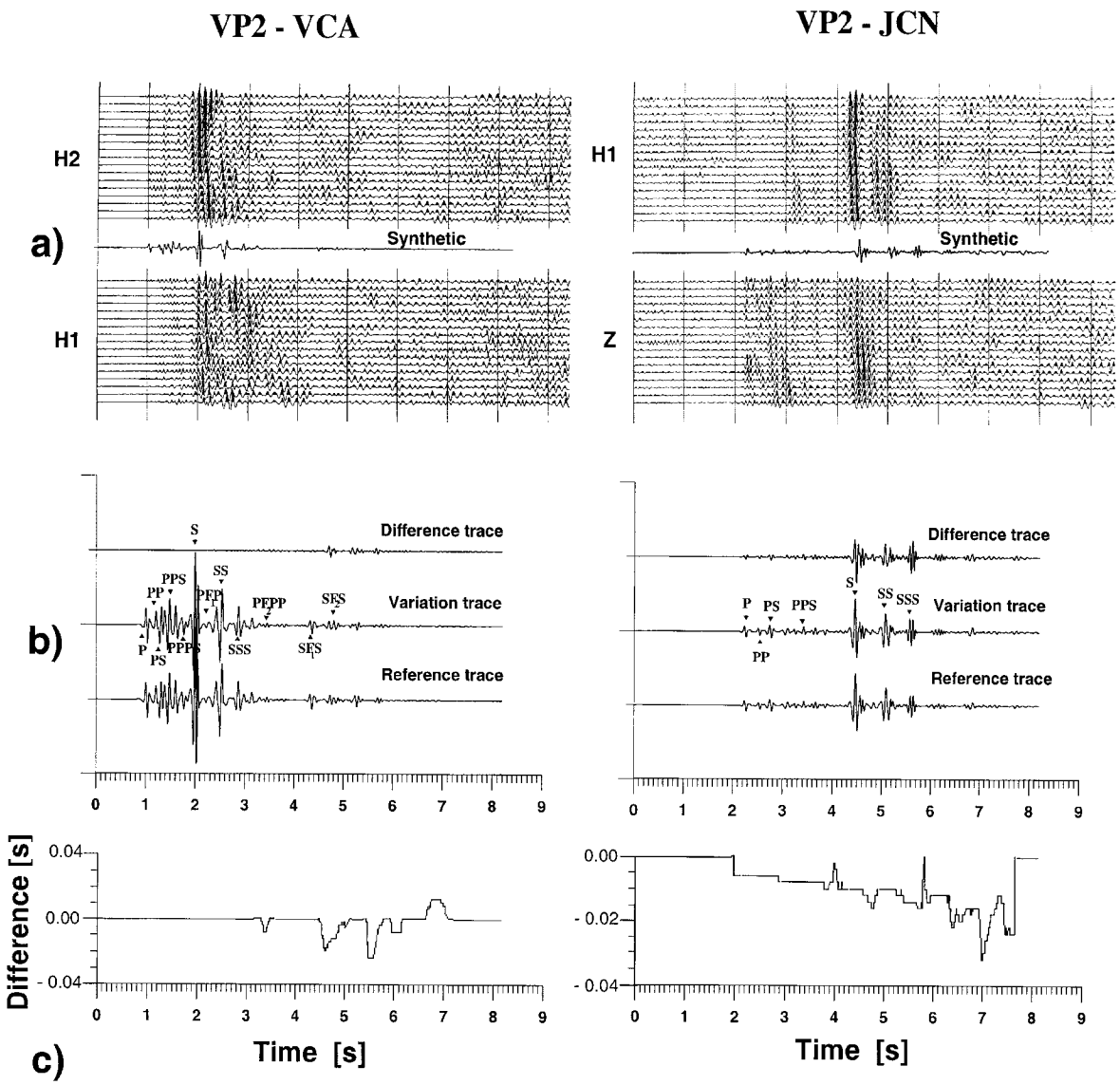

Figure 3. Travel-time anomaly produced by a 6% velocity increase within the fault zone. (a) Comparisons of observed seismograms from the VCA source array (fault-normal horizontal source, ground-motion components as indicated in Figure 2) with fault-normal horizontal-component synthetic seismograms (central traces) at VCA and JCN. (b) Effects on the seismograms of a 6% velocity increase in the fault zone. Lower trace is the reference velocity model (see Figure 2); middle trace is for the velocity increase in the fault zone; upper traces show differences between the two seismograms that will produce travel-time changes when the traces are cross-correlated. (c) Travel-time variations along the seismograms, as determined by the cross-correlation method of Karageorgi *et al.* (1992). At VCA variations start after arrival of the fault-zone reflections, while at JCN they begin with the initial *P* wave and increase in magnitude as more *S*-wave energy becomes involved.

Summary and Conclusions

Karageorgi *et al.* (1997) demonstrate convincingly that they indeed detected real changes in travel times in their eight-year controlled-source monitoring program at Parkfield. They localized the anomalous changes to a region southeastward from Middle Mountain, roughly in the presumed nucleation zone for the past and future *M* 6 Parkfield earthquakes. Their best hypothesis for the phenomenon called for changing fluid conditions in the shallow section above the fault zone. Our study supports that hypothesis and offers a more quantitative model for the actual wave propagation involved. The remaining link in the puzzle lies in

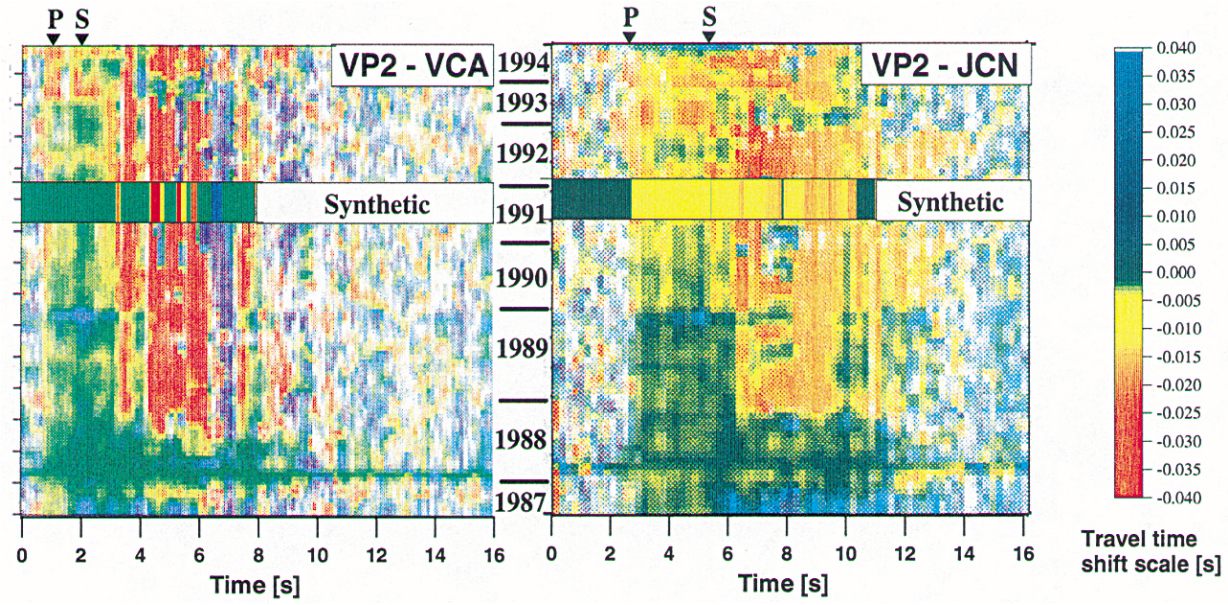

Figure 4. Comparison of calculated travel-time changes for 6% velocity increase in the fault zone to the history of changes for paths VP2 to VCA and JCN from Karageorgi *et al.* (1997). The small strips present the computed travel-time changes from Figure 3 at the same color scale. The match is very good, and the contrasting effects within the *P*-to-*S* interval on opposite sides of the fault localizes the changing medium to the fault zone. Color intensity in the monitoring data is reduced with decreasing signal coherence along the seismogram.

the responsible mechanism for the velocity change in the fault zone. We are inclined to accept the idea of a deeper tectonic deformation, perhaps the slip-rate transients identified by Nadeau and McEvilly (1999) and Silver *et al.* (1999), that somehow changed the fluid environment in the shallow fault zone, producing these effects that are not seen in deeper wave propagation from microearthquakes.

The striking importance of the shallow vertical velocity gradient cannot be overstated. It is clear from this study that surface sources employed in highly heterogeneous environments such as the San Andreas fault zone can be expected to generate an overwhelming near-surface wave field that must be dealt with in looking for deeper images. If the individual phases can be identified, however, they may provide an important tool for studying near-surface details of the fault-zone structure.

Acknowledgments

The Parkfield High-Resolution Seismic Network functions through close cooperation among scientists from the University of California at Berkeley, Lawrence Berkeley National Laboratory (LBNL) and the U.S. Geological Survey (USGS). The USGS provided financial support for this research through NEHRP award 1434-95-G-2540; however, these results do not necessarily represent official government policies. Rich Clymer manages the field operations at Parkfield and the shear vibrator used in this study, donated by Amoco to U.C. Berkeley, is operated and maintained by Don Lippert at the Geophysical Measurements Facility (GMF) at LBNL. Data processing was done at the Center for Computational Seismology (CCS) at LBNL, which is operated by the University of California for the U.S. Department of Energy (DOE) under contract No. DE-AC03-76SF00098. CCS and GMF have been supported specifically by the DOE Office of Basic Energy Sciences.

References

Antolik, M., R. M. Nadeau, R. C. Aster, and T. V. McEvilly (1996). Differential analysis of coda Q using similar microearthquakes in seismic gaps, part 2: application to seismograms recorded by the Parkfield High Resolution Seismic Network, *Bull. Seism. Soc. Am.* **86,** 890–910.

Bakun, W. H., and A. G. Lindh (1985). The Parkfield, California, prediction experiment, Earthquake Predict. Res. **3,** 285–304.

Cao, S., and S. Greenhalgh (1992). Finite-difference simulation of *P-SV*-wave propagation: a displacement potential approach, *Geophys. J. Int.* **109,** 525–535.

Eberhart-Phillips, D., and A. J. Michael (1993). Three-dimensional velocity structure, seismicity, and fault structure in the Parkfield region, central California, *J. Geophys. Res.* **98,** 1153–1172.

Karageorgi, E., R. Clymer, and T. V. McEvilly (1992). Seismological studies at Parkfield. II: search for temporal variations in wave propagation using Vibroseis *Bull. Seism. Soc. Am.* **82,** 1388–1415.

Karageorgi, E. D., T. V. McEvilly, and R. W. Clymer (1997). Seismological studies at Parkfield IV: variations in controlled-source waveform parameters and their correlation with seismic activity, 1987–1994, *Bull. Seism. Soc. Am.* **87,** 39–49.

Korneev, V. A., R. M. Nadeau, T. V. McEvilly, and E. Karageorgi (1998). Characteristics of wave propagation in the San Andreas fault-zone at Parkfield: observations and modeling, *EOS* **79,** 583.

Li, Y.-G., W. L. Ellsworth, C. H. Thurber, P. E. Malin, and K. Aki (1997). Fault-zone guided waves from explosions in the San Andreas fault at Parkfield and Cienega Valley, California, *Bull. Seism. Soc. Am.* **87,** 210–221.

Michelini, A., and T. V. McEvilly (1991). Seismological studies at Parkfield: I. simultaneous inversion for velocity structure and hypocenters using B-splines parameterization, *Bull. Seism. Soc. Am.* **81,** 524–552.

Nadeau, R. M., and T. V. McEvilly (1999). Fault slip rates at depth from recurrence intervals of repeating microearthquakes, *Science* **285,** 718–721.

Nadeau, R., M. Antolik, P. Johnson, W. Foxall, and T. V. McEvilly (1994a). Seismological studies at Parkfield III: microearthquake clusters in the study of fault-zone dynamics, *Bull. Seism. Soc. Am.* **83,** 247–263.

Nadeau, R. M., E. D. Karageorgi, and T. V. McEvilly (1994b). Fault-zone monitoring with repeating similar microearthquakes: a search for the Vibroseis anomaly at Parkfield, *Seism. Res. Lett.,* **65,** 69.

Sieh, K. E., Central California foreshocks of the great 1857 earthquake (1978). *Bull. Seism. Soc. Am.* **68,** 1731–1749.

Silver, P. G., S. S. Gao, and A. T. Linde (1999). Characterization of the Parkfield transient: evidence for aseismic stress transfer, *EOS* **80,** F691.

Center for Computational Seismology
Lawrence Berkeley National Laboratory
(V. A. K., T. V. M., E. D. K.)

Berkeley Seismological Laboratory
University of California, Berkeley, California, 94720
(T. V. M.)

Enterprise Oil Exploration Limited
Maroussi 151 25 Athens
Greece
(E. D. K.)

Manuscript received 15 April 1999.